Frequency-Domain Substructure Isolation
for Local Damage Identification

by

Jilin Hou, Lukasz Jankowski and Jinping Ou

Reprinted from

Advances in Structural Engineering

Volume 18 No. 1 2015

MULTI-SCIENCE PUBLISHING CO. LTD.
26 Eldon Way, Hockley, Essex SS5 4AD, United Kingdom

Frequency-Domain Substructure Isolation for Local Damage Identification

Jilin Hou[1,*], Łukasz Jankowski[2] and Jinping Ou[1,3]

[1]School of Civil Engineering, Dalian University of Technology, Dalian 116024, China
[2]Institute of Fundamental Technological Research, Polish Academy of Sciences, Warsaw, Poland
[3]School of Civil Engineering, Harbin Institute of Technology, Harbin 150090, China

(Received: 2 March 2014; Received revised form: 30 July 2014; Accepted: 20 August 2014)

Abstract: This paper proposes a frequency-domain method of substructure identification for local health monitoring using substructure isolation method (SIM). The first key step of SIM is the numerical construction of the isolated substructure, which is a virtual and independent structure that has the same physical parameters as the real substructure. Damage identification and local monitoring can be then performed using the responses of the simple isolated substructure and any of the classical methods aimed originally at global structural analysis. This paper extends the SIM to frequency domain, which allows the computational efficiency of the method to be significantly increased in comparison to time domain. The mass-spring numerical model is used to introduce the method. Two aluminum beams with the same substructure are then used in experimental verification. In both cases the method performs efficiently and accurately.

Key words: structural health monitoring (SHM), damage identification, substructuring, frequency domain, boundary.

1. INTRODUCTION

Structural Health Monitoring (SHM) has become a hot and intensively researched field in civil engineering: monitoring and damage identification play important roles in maintaining integrity and safety of structures (Yi *et al*. 2012; Zhou, Yan, Wang and Ou 2013). Many effective methods have been proposed for damage identification (Fan and Qiao 2011; Moragaspitiya *et al*. 2012; Wang *et al*. 2013; Zhou, Yan and Ou 2013). However, accurate global identification of large real-world structures is not easy due to their complex and often unknown boundary conditions, temperature effect (Xia *et al*. 2012) , nonlinear components, small sensitivity of global response to localized damages, etc. Furthermore, global identification (parameter identification of the global structure) often involves large numbers of unknowns and sensors. This is costly, rarely feasible in practice, and usually yields severely ill-conditioned identification problems. The substructuring approach seems to be a possible solution. At present, there are two main kinds of substructuring methods that can be applied to substructure identification: (1) Mechanical substructuring/coupling methods (MSC methods), which assemble dynamic characteristics of the global structure from known dynamic characteristics of all its substructures. In applications to substructural monitoring, the global structure is first separated into several independent substructures, and then dynamic tests and identification are performed separately on each substructure. The substructures are then coupled back into the global structure via displacement coordination on the interface (Ewins 2000, 469-499; Maia and Silva 1997, 265-302). (2) Substructuring/decoupling methods (SD methods), whose purpose is to decouple an unknown substructure from an unknown global structure for the purpose of

*Corresponding author. Email address: houjilin@dlut.edu.cn; Fax: +8641184706432; Tel: +8641184706427.

local substructural monitoring or identification. To this end, first a local dynamic test is performed on the global structure, and then the local substructure is analyzed by taking into account the interaction between it and the global structure. Methods of this kind do not separate the substructure from the global structure during the test (Tee *et al*. 2005). The MSC methods are usually used in mechanical or aerospace field. For structures in civil engineering, only the response of a global structure can be obtained during its service period and it is impossible to mechanically separate its substructures. Therefore most existing substructural approaches for structures in civil engineering are substructuring/decoupling (SD) methods. The method proposed in this paper belongs thus to SD methods. Such methods can focus on local small substructures; they need only a few sensors placed on the substructure and yield smaller and numerically much more feasible identification problems.

To detect and locate the substructural damage, one can compare locally sensitive information obtained before and after damage. For example, Yun and Bahng (2000) used natural frequencies and mode shapes for local monitoring of stiffness modifications. Bao *et al*. (2012) used the damage basic probability assignment (BPA) function of substructures for preliminary damage localization. An and Ou (2013) presented a model updating method that utilizes four cost functions involving free vibration accelerations and local mode shapes to detect local damage of a truss structure.

A substructure is a local part of the global structure, and so it is not independent of the global structure. In order to focus on the substructure only, most existing SD methods separate the substructure from the global structure; the interface forces are then used for coupling both structures and need to be identified together with substructural parameters. The identification is performed mostly based on the equation of motion of the substructure. Koh *et al*. (2003) employed genetic algorithms (GA) as the search tool for its advantages including the ease of implementation and the desirable characteristics of global search. Tee *et al*. (2005) developed a divide-and-conquer approach for identification at the substructural level of first-order and second-order models. Law *et al*. (2010) identified the coupling forces between substructures using the damped least-squares method. Wang *et al*. (2011) employed the concept of the "quasi-static displacement" vector to simplify the interface forces, and use a GA method to identify the substructure. A multi-feature GA method was used by Trinh and Koh (2012) to estimate substructural mass, damping and stiffness parameters. Xing and Mita (2012) confine each substructure of a multi-storey shear building to a few degrees of freedom only (Dofs) and use overlapping substructures, then they apply directly the ARMAX method for identification. Zhu *et al*. (2013) identify the structural damage, the external moving force and interface forces of adjacent substructures simultaneously from the measured dynamic acceleration responses. The above methods are formulated in time domain. There are also many studies of substructure identification in frequency domain. In order to avoid the need for complete instrumentation of the substructure, Yuen and Katafygiotis (2006) presented an output-only bayesian frequency-domain approach for substructure identification and monitoring in linear MDOF systems. Tee *et al*. (2009) use System Equivalent Reduction Expansion Process to condense the sub-model for substructural identification. Zhang *et al*. (2010) introduced a control system to identify storey parameters in a shear structure using Cross Power Spectral Density (CPSD). Xia *et al*. (2010) developed Kron's substructuring method to compute the first-order derivatives of the eigenvalues and eigenvectors.

The substructure and the global structure remain coupled by the unknown interface forces that are exposed on the separated substructural interface. As these forces influence substructural responses, the methods used for substructure identification are very different from the methods of global identification, which cannot be directly applied to the substructure in all their variety and flexibility. Damage of the global structure can be detected by direct signal processing of the constructed response using time series methods (Nair *et al*. 2003) or wavelet analysis (Rucka and Wilde 2010), or be estimated by optimizing the finite element (FE) model of the substructure using its flexibility matrix (Duan *et al*. 2005), natural frequencies and mode shapes (Hassiotis 2000), time-domain response (Suwała and Jankowski 2012) or frequency-domain response (Lin and Ewins 1990), etc.

Hou *et al*. (2012) have proposed the Substructure Isolation Method (SIM), where the isolated substructure is an independent structure and all global identification methods can be applied to its identification. The SIM proceeds in two stages. First, in the isolation stage, measured responses are directly utilized to construct the responses of the isolated substructure, which is an independent virtual structure with the same structural parameters as the real substructure, but isolated from the global structure with virtual supports placed on the interface. Then, in the identification stage, local identification of the substructure is performed based on the constructed responses of the isolated substructure

and any of the standard methods aimed originally at global identification. The selection of the identification method usually depends on the characteristics of the constructed responses of the isolated substructure. This paper uses natural frequencies to optimize the substructure.

In the original formulation of the SIM (Hou *et al*. 2012), the isolated substructure and its responses were constructed in time domain. It involved computing a solution to a very large and extremely ill-conditioned discrete linear system, which originated from a discretization of a system of Volterra integral equations of the first kind and had the dimensions proportional to the number of the considered time steps. Solution of such a system is time-consuming, which significantly limited the manageable measurement time interval. This paper formulates the SIM in frequency domain, which dramatically improves its computational efficiency: even though significantly longer measurement time intervals are used, the method performs much faster. The next section derives the SIM using frequency-domain responses. Section 3 makes use of a simple mass-spring system to introduce the application of the method. The last section verifies experimentally the proposed approach using an aluminum cantilever beam.

2. SUBSTRUCTURE ISOLATION METHOD IN FREQUENCY DOMAIN (SIM-FD)

2.1. Construction of the Isolated Substructure

Denote by $x(t)$ the vector of displacements in all Dofs of the global structure, and by **M, C** and **K** the corresponding mass, stiffness, and damping matrices. It is assumed that the Eqn of motion in time domain can be written as:

$$Mx(t) + Cx(t) + Kx(t) = f(t) \tag{1}$$

where the vector $f(t)$ collects all the external excitations. The Fourier transform $\mathcal{F}$, applied to both sides of (1), yields the frequency-domain quasi-static form of the equation of motion:

$$\left(-\omega^2 \mathrm{M} + \mathrm{j}\omega \mathrm{C} + \mathrm{K}\right) X(\omega) = F(\omega) \tag{2}$$

where $X(\omega) = (\mathcal{F}x)(\omega)$ and $(F)(\omega) = (\mathcal{F}f)(\omega)$ Let the subscript "s" denote the Dofs internal to the substructure, "b" the Dofs of its interface and "r" all the Dofs outside the substructure. Henceforth, these subscripts will be used to mark the corresponding blocks of system matrices and the corresponding parts of response and excitation vectors. Eqn can be thus stated in the equivalent form,

$$\begin{bmatrix} \left(-\omega^2 \begin{bmatrix} \mathrm{M_{ss}} & \mathrm{M_{sb}} & 0 \\ \mathrm{M_{bs}} & \mathrm{M_{bb}} & \mathrm{M_{br}} \\ 0 & \mathrm{M_{rb}} & \mathrm{M_{rr}} \end{bmatrix} + \right. \\ \left. \mathrm{j}\omega \begin{bmatrix} \mathrm{C_{ss}} & \mathrm{C_{sb}} & 0 \\ \mathrm{C_{bs}} & \mathrm{C_{bb}} & \mathrm{C_{br}} \\ 0 & \mathrm{C_{rb}} & \mathrm{C_{rr}} \end{bmatrix} + \begin{bmatrix} \mathrm{K_{ss}} & \mathrm{K_{sb}} & 0 \\ \mathrm{K_{bs}} & \mathrm{K_{bb}} & \mathrm{K_{br}} \\ 0 & \mathrm{K_{rb}} & \mathrm{K_{rr}} \end{bmatrix} \right) \\ \begin{bmatrix} X_{\mathrm{s}}(\omega) \\ X_{\mathrm{b}}(\omega) \\ X_{\mathrm{r}}(\omega) \end{bmatrix} = \begin{bmatrix} F_{\mathrm{s}}(\omega) \\ F_{\mathrm{b}}(\omega) \\ F_{\mathrm{r}}(\omega) \end{bmatrix} \end{bmatrix} \tag{3}$$

Assume that $n+1$ external excitations $F^0(\omega)$, $F^1(\omega)$, …, $F^n(\omega)$ are applied to the structure and let $X^0(\omega)$, $X^1(\omega)$, …, $X^n(\omega)$ be the corresponding responses. Denote by $P(\omega)$ the following linear combination of the excitations:

$$P(\omega) = F^0(\omega) + \sum_{i=1}^{n} Z^{\mathrm{i}}(\omega) F^{\mathrm{i}}(\omega), \tag{4}$$

where $Z^{\mathrm{i}}(\omega)$ are arbitrary complex combination coefficients. Let $Y(\omega)$ denote the corresponding structural response, which is a similar combination that can be stated separately for internal and interface Dofs as

$$\begin{aligned} &Y_{\mathrm{s}}(\omega) = X_{\mathrm{s}}^0(\omega) + \\ &\sum_{i=1}^{n} Z^i(\omega) X_{\mathrm{s}}^i(\omega) = X_{\mathrm{s}}^0(\omega) + D(\omega) Z(\omega), \\ &Y_{\mathrm{b}}(\omega) = X_{\mathrm{b}}^0(\omega) + \\ &\sum_{i=1}^{n} Z^i(\omega) X_{\mathrm{b}}^i(\omega) = X_{\mathrm{b}}^0(\omega) + \mathrm{B}(\omega) Z(\omega), \end{aligned} \tag{5}$$

where the matrices $\mathrm{D}(\omega)$ and $\mathrm{B}(\omega)$ are composed of the respective responses of the internal and interface Dofs and the vector $Z(\omega)$ collects the combination coefficients,

$$\begin{aligned} Z(\omega) &= \left[Z_1(\omega) \cdots Z_n(\omega) \right]^{\mathrm{T}}, \\ \mathrm{D}(\omega) &= \left[X_{\mathrm{s}}^1(\omega) \cdots X_{\mathrm{s}}^{\mathrm{n}}(\omega) \right], \\ \mathrm{B}(\omega) &= \left[X_{\mathrm{b}}^1(\omega) \cdots X_{\mathrm{b}}^{\mathrm{n}}(\omega) \right]. \end{aligned} \tag{6}$$

For the reasons described in Section 2.3, $F^0(\omega)$is called the *basic excitation*, and the corresponding response $X^0(\omega)$ is the *basic response*; $F^1(\omega)$, …, $F^n(\omega)$, are the *constraining excitations*, and the corresponding

responses $X^1(\omega)$, …, $X^n(\omega)$, are the *constraining responses*. Correspondingly, the matrices and $B(\omega)$, $D(\omega)$ are called the *constraining matrices*.

Since the substructure is assumed to be linear, the linearly combined excitation $P(\omega)$ and the linearly combined response $Y(\omega)$ satisfy together the equation of motion (see Eqn 3). The first row of this equation can be then written as

$$\left(-\omega^2 \mathrm{M}_{ss} + \mathrm{j}\omega \mathrm{C}_{ss} + \mathrm{K}_{ss}\right) Y_s(\omega) = P_s(\omega) + P_c(\omega), \quad (7)$$

where

$$P_c(\omega) = -\left(-\omega^2 \mathrm{M}_{sb} + \mathrm{j}\omega \mathrm{C}_{sb} + \mathrm{K}_{sb}\right) Y_b(\omega) \quad (8)$$

is the vector of the interface forces that couple the substructure to the outside structure via the interface Dofs. If the combined responses of the substructure interface vanish, $Y_b(\omega) = 0$, then the coupling interface forces $P_c(\omega)$ also vanish, and Eqn 7 is simplified into

$$\left(-\omega^2 \mathrm{M}_{ss} + \mathrm{j}\omega \mathrm{C}_{ss} + \mathrm{K}_{ss}\right) Y_s(\omega) = P_s(\omega) \quad (9)$$

According to the second equation of Eqn, the combined interface responses $Y_b(\omega)$ vanish and Eqn (9) holds, if the combination coefficients $Z(\omega)$ satisfy

$$0 = X_b^0(\omega) + \mathrm{B}(\omega) Z(\omega) \quad (10)$$

Eqn (10) is a linear equation that is uniquely solvable if the matrix $B(\omega)$ has full column rank, which is possible only if the number n of the constraining excitations/responses is not smaller than the number of the interface Dofs. The solution is given by

$$Z(\omega) = -\left[\mathrm{B}(\omega)\right]^+ X_h^0(\omega) \quad (11)$$

where the superscript "+" denotes the pseudo-inverse of a matrix. The corresponding combined response of the substructure can be then stated in the explicit form as

$$Y_s(\omega) = X_s^0(\omega) - \mathrm{D}(\omega)\left[\mathrm{B}(\omega)\right]^+ X_b^0(\omega) \quad (12)$$

In the above analysis, the combination coefficients are chosen in such a way that the combined response of the substructure interface vanish. This is equivalent to adding fixed supports in all Dofs of the interface and thus to full isolation of the substructure from the global structure. In other words: given the properly linearly combined excitation $P_s(\omega)$, the coupling interface forces $P_c(\omega)$ vanish and the substructure responds with $Y_s(\omega)$ as an independent structure, see Eqn 9. Notice that the excitation $P_c(\omega)$ and the response $Y_s(\omega)$ are not directly measured, but rather artificially constructed from measured data. Hence, the constructed system is not physical but virtual. Such an independent virtual substructure is called the *isolated substructure*. It is isolated from the outside structure by adding fixed virtual supports in all Dofs of their interface.

The above approach requires the responses to be measured in all Dofs of substructure interface. Therefore, it is hardly applicable to substructures with a large number of interface Dofs. The proposed method needs thus a proper selection of the substructure, so that it has a simple interface. However, the identification of the isolated substructure can be performed using standard methods of global identification, and so there is no similar limitation imposed on the interior of the substructure, which can be complex with a large number of Dofs.

2.2. The Virtual Support and Other Types of Sensors

In the previous section, all the responses are assumed to be displacement in substructural and interface Dofs. Consequently, the frequency response of the isolated substructure is derived based on fixed virtual supports. In fact, other kinds of virtual supports can be also used to emulate other types of boundary conditions, depending on the type of the substructure and sensors placed on its interface. In the following, isolation of a plane beam is used as an illustrative example. Figure 1 shows the exposed interface of the substructure. For the sake of simplicity, the axial displacement of the neutral axis and the axial force are ignored for the moment. The following physical quantities are of interest on the interface: the internal shear force $p(t)$ and bending moment $M(t)$, the vertical displacement $v(t)$, the rotation $\theta(t)$ and the axial strain $\varepsilon(t)$ of the beam surface. Notice that, in the absence of axial displacement and force, the strain $\varepsilon(t)$ is proportional to the bending moment, but much easier to measure. Four different types of boundary conditions can be now formulated,

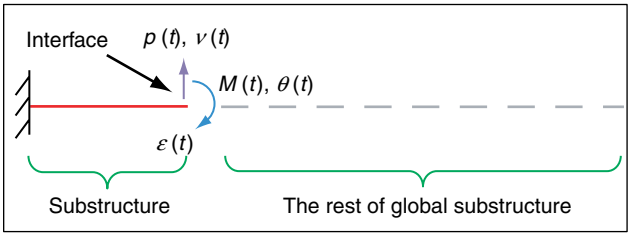

Figure 1. A beam substructure

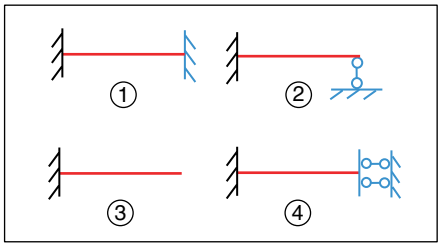

Figure 2. Four types of virtual supports

$$①\begin{cases} v(t)=0 \\ \theta(t)=0 \end{cases} ②\begin{cases} v(t)=0 \\ \varepsilon(t)=0 \end{cases} ③\begin{cases} p(t)=0 \\ \varepsilon(t)=0 \end{cases} ④\begin{cases} p(t)=0 \\ \theta(t)=0 \end{cases} \tag{13}$$

which define four kinds of virtual supports that can be applied in the interface to isolate the substructure, see Figure 2.

In practice, it is usually impossible to place physical supports or apply the proper loads to make the interface responses satisfy one of the four conditions listed in Eqn 13. However, Section 2.1 shows that a number of nonzero interface responses can be linearly combined to zero, so that the combined response satisfies the boundary conditions. As a result, the type of the virtual support depends on the types of interface sensors. For instance, if $v(t)$ and $\theta(t)$ are measured, then the virtual fixed support ① can be constructed by a linear combination of the measured responses. Or, if responses $v(t)$ and $\varepsilon(t)$ are measured, the virtual pined support ② can be constructed. In real applications, the shear force $p(t)$ is hard to measure, so that the 3rd and 4th kind of virtual supports will be usually not used.

As in Section 2.1, assume that there are n+1 excitations and denote the corresponding responses by $X_{\mathrm{s}}^0(\omega), X_{\mathrm{s}}^1(\omega), \ldots, X_{\mathrm{s}}^n(\omega)$ for the interface sensors (that need to be compliant in type with one of) and by $X_{\mathrm{b}}^0(\omega), X_{\mathrm{b}}^1(\omega), \ldots, X_{\mathrm{b}}^n(\omega)$ for the sensors placed inside the substructure. The substructure and all the sensors are linear, so that Eqns 4 to 6 hold. As a result, Eqn (10) can be solved to find the combination coefficients that make the combined response satisfy the boundary conditions. Finally, the corresponding combined response of the isolated substructure is given by Eqn 12. Notice that for a complete isolation, Eqn 10 needs to be exactly satisfied, which means that B(ω) must be of full row rank. Rows of B(ω) correspond to interface sensors and its columns to combination coefficients $Z^i(\omega)$, and hence the number n of constraining excitations/responses must not be smaller than the number of the interface sensors.

If axial displacement of the neutral axis of the beam and axial force are to be considered, the strain $\varepsilon(t)$ of the surface of the beam is no longer a direct substitute for the internal bending moment. In such a case, two strain sensors can be placed on the opposite faces of the beam in the same distance from its neutral axis: the axial stress and the bending moment will be proportional to the sum and to the difference of their measurements, respectively.

2.3. Local Damage Identification

Local identification of substructure damages is equivalent to damage identification of the isolated substructure, which is an independent system that has its own natural frequencies and mode shapes that can be found by investigation of the constructed response $Y_{\mathrm{s}}(\omega)$ and the corresponding combined excitation $P_{\mathrm{s}}(\omega)$ of the isolated substructure,

$$P_{\mathrm{s}}(\omega) = F_{\mathrm{s}}^0(\omega) + \sum_{i=1}^{n} Z^i(\omega) F_{\mathrm{s}}^i(\omega) \tag{14}$$

where $F_{\mathrm{s}}^i(\omega)$ is the part of the vector $F^i(\omega)$ that corresponds to the internal Dofs of the substructure, see Eqn 4, and the combination coefficients are given by Eqn 11 to ensure proper isolation.

As a result, local damage identification can be performed by optimizing a vector μ of certain parameters in the FE model of the isolated substructure that are assumed to quantify the damage. Specific meaning of the parameters is application-dependent (e.g., stiffness modification ratios). The optimization can be performed by any of the classical methods that have been originally aimed at global identification. Selection of a particular method depends on characteristics of the constructed response, which is dependent on the combined excitation $P_{\mathrm{s}}(\omega)$ of the isolated substructure. The combined excitation is particularly easy to find, if $F_{\mathrm{s}}^i(\omega) = 0$ for $i = 1, \ldots, n$, that is if all the constraining excitations are applied on the interface or outside the substructure. In such a case, the combined excitation of the substructure equals its basic excitation $F_{\mathrm{s}}^0(\omega)$. The combined response $Y_{\mathrm{s}}(\omega)$ is then the response of the isolated substructure to the basic excitation only.

In this paper, a modal hammer is used as the excitation in experiment. This is a quasi-impulsive excitation with a broad spectrum that excites many natural frequencies of the isolated substructure. The vector μ of damage parameters is identified by minimizing the following objective function

$$\Delta(\mu) = \sum_i \left| \frac{\omega_i^F(\mu) - \omega_i^{\mathrm{m}}}{\omega_i^{\mathrm{m}}} \right|^2 \tag{15}$$

where ω_i^{m} is the ith identified natural frequency of the isolated substructure and $\omega_i^{\mathrm{F}}(\mu)$ denotes the natural frequencies of its FE model;

2.4. Fast Fourier Transform (FFT) of the Response

In real applications the measured response is discrete, so the Fast Fourier Transform (FFT) needs to be used to compute the frequency response. When the time-domain signal is of a finite length and does not tend to zero in the integration time, spectral leakage is inevitable (Harris 1979). It can significantly affect the accuracy of the frequency response constructed in Eqn. To minimize its effects, the windowing process is employed during the FFT. This paper tests the exponential window $w_{\mathrm{e}}(t;\eta)$ and the Hanning window $w_{\mathrm{h}}(t)$,

$$w_{\mathrm{e}}(t;\eta)=\begin{cases}\mathrm{e}^{-\eta t} & \text{for } 0\le t\le T,\\ 0 & \text{elsewhere,}\end{cases} \tag{16}$$

$$w_{\mathrm{h}}(t)=\begin{cases}\dfrac{1}{2}+\dfrac{1}{2}\cos\left(\dfrac{\pi t}{T}\right) & \text{for } 0\le t\le T,\\ 0 & \text{elsewhere,}\end{cases} \tag{17}$$

where η denotes the decay rate of the exponential window and T denotes the measurement time interval. The Fourier transform with the exponential windows is equivalent to the Laplace transform, $F\left[\mathrm{e}^{-\eta t}x(t)\right](\omega)=L\left[x(t)\right](s)$, where L is the Laplace operator and $s = j\omega + \eta$. If the exponential window is used, Eqn (12) should be stated as

$$Y_{\mathrm{s}}(s)=X_{\mathrm{s}}^{0}(s)-\mathrm{D}(s)\left[\mathrm{B}(s)\right]^{+}X_{\mathrm{b}}^{0}(s), \tag{18}$$

A useful feature of the exponential window can be considered to support its feasibility. Compare the free response of an n-Dofs structure with the same response after windowing,

$$x(t)=\sum_i A_i\phi_i\mathrm{e}^{-\omega_i\xi_i\tau}\sin\left(\omega_{di}t+\varphi_i\right),$$

$$x(t)w_{\mathrm{e}}(t;\eta)=\sum_i A_i\phi_i\mathrm{e}^{-\omega_i\left(\xi_i+\frac{\eta}{\omega_i}\right)\tau}\sin\left(\omega_{di}t+\varphi_i\right), \tag{19}$$

where ϕ_i is the shape of the ith mode, ω_i is the ith natural frequency, ξ_i is the damping ratio, and $\omega_{di}=\omega_i\left(1-\xi_i^2\right)^{0.5}$. The exponential window increases the damping ratio of the free response by η/ω_i and does not change its frequency content, which is unlike other windows including the Hanning window.

2.5. Isolation in Frequency Domain vs. Isolation in Time Domain

Isolation in time domain (Hou *et al*. 2012) (SIM-TD) and in frequency domain (SIM-FD) are both based on the same concept: the substructure is isolated from the global structure into an independent structure by adding virtual supports on its interface. The time-domain counterpart of Eqn (10) and the corresponding formula for the response of the isolated substructure are

$$\begin{cases}0=x_{\mathrm{b}}^{0}(t)+\sum_{i=1}^{n}\int_0^t x_{\mathrm{b}}^{i}(t-\tau)z_i(\tau)d\tau,\\ Y_{\mathrm{s}}(t)=x_{\mathrm{s}}^{0}(t)+\sum_{i=1}^{n}\int_0^t x_{\mathrm{s}}^{i}(t-\tau)z_i(\tau)d\tau.\end{cases} \tag{20}$$

During the isolation process the first equation is solved to find the functions $z_i(t)$, which are then substituted into the second equation to find the response of the isolated substructure. The first equation is a system of Volterra integral equations of the first kind (Kress 1989). The advantages and disadvantages of the time- and frequency-domain approaches can be summarized as follows:

1) The SIM-TD directly uses the measured time-domain responses, so that it avoids the errors related to the Fourier transform. However, the computations extensively employ time-consuming convolutions and require solving a discretized version of a system of Volterra integral equations of the first kind, which is an extremely ill-conditioned problem that requires numerical regularization techniques.

2) In the SIM-FD, the computational effort is significantly reduced, as all the convolutions are efficiently performed in frequency domain. The computations can be focused on a selected frequency range only, which further reduces the computational time. As a result, a larger number of responses measured in a longer time interval can be used. However, the SIM-FD approach may introduce inaccuracies related to the FFT and spectral leakage.

3. NUMERICAL EXAMPLE

This section uses a mass-spring system for initial verification of the proposed isolation method in frequency domain.

3.1. Six-Dof Mass-Spring System

The mass-spring system is a 6-Dof structure shown in Figure 3(a). The stiffness of each floor is k = 2 kN/m; all the lumped masses are m = 4 kg. The 1st and 2nd order damping ratios are 1%. The substructure consists of the 4th, 5th and 6th mass, see Figure 3(b).

3.2. Excitations, Sensors and the FRF (Frequency Response Function)

Assume that two acceleration sensors are used, X3 and X5, placed respectively on the 3rd and 5th mass. Assume also that two impulse excitations, F3 and F6, can be applied respectively to the 3rd and 6th mass. Altogether four responses (denoted Xi-Fj) are simulated; they correspond to the four terms used in Eqn 12 to construct the response of the isolated substructure, see Table 1.

Figure 4 plots the simulated FRFs of the global system. They are directly used in Eqn 12 to construct the FRF of the isolated substructure. The result is compared in Figure 5 to the accurate frequency response computed using the FE model of the substructure. The response obtained using the SIM is the same as that directly computed, which confirms that the isolated substructure can be constructed successfully. The stars in Figure 5, as well as in Figures 8 to 11, mark the accurate natural frequencies computed using the FE model of the isolated substructure.

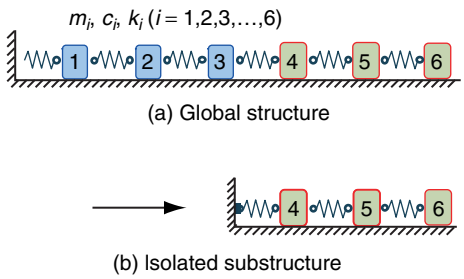

Figure 3. A 6-Dof mass-spring system

Table 1. Excitations and responses

	Excitations	
Sensors	**Constraining F3**	**Basic F6**
Interface X3	X3-F3: $B(\omega)$	X3-F6: $X_b^0(\omega)$
Internal X5	X5-F3: $B(\omega)$	X5-F6: $X_s^0(\omega)$

3.3. Windowing and the FFT

In order to simulate a real application with time-domain excitations, a simulated hammer excitation is applied at F3 and F6, see Figure 6. The responses of the global structure are shown in Figure 7. The sampling frequency is 200 Hz and the time interval is T = 2.56s.

Three windowing functions are used to decrease the spectral leakage: no windowing, the exponential window (Eqn 16) and the Hanning window (Eqn 17). In order to increase the frequency resolution of the FFT, several zeros are added in front of the windowed responses (the measurement time interval is increased eightfold and filled with zeros at the beginning). The results of the FFT are used in Eqn 12 to construct the FRF of the isolated substructure. Figure 8 to Figure 10 compare the FRF constructed using the SIM to the actual FRF computed using the FE model. The theoretical FRF is smooth, and peaks appear only around structural frequencies. But due to truncation of the measured response in time domain, there is spectral leakage in its computed fast Fourier transform, so that the computed FRF is not smooth and has many small peaks, see Figure 8 (No-FEM). For this reason, the isolated substructure constructed using such a frequency response cannot provide reliable modal information, see Figure 8 (No-SIM). It can be seen that only the exponential window (Figure 9) can lead to consistent results, provided the window decay rate is properly selected. Even if the Hanning window (Figure 10) yields almost the same positions of the peaks, the amplitudes deviate significantly. As mentioned in Section 2.4, the exponential window only increases the damping ratio of the free response and does not change its frequency content, which is unlike other windows including the Hanning window. Therefore, the exponential window is selected in the method.

The exponential window increases the effective system damping. Thus, the constructed FRF depends on the window decay rate η or, alternatively, on the attenuation ratio r at the end of time interval T, which are related to each other by

$$\eta = -\frac{\ln r}{T}. \tag{21}$$

Four exemplary values of the parameter r are tested to construct the FRF of the isolated substructure, see

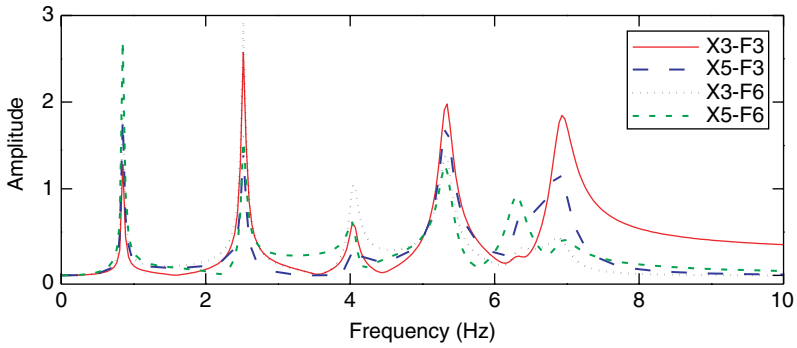

Figure 4. FRFs of the global structure

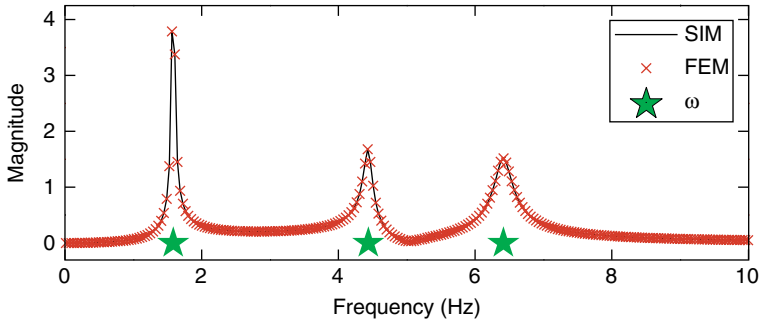

Figure 5. FRF of the isolated substructure

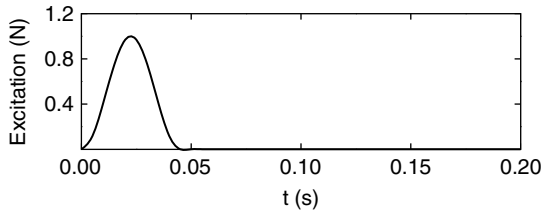

Figure 6. Simulated hammer excitation

Figure 11. For r = 1e-1, there are two peaks near the first natural frequency, which might suggest that 1e-1 is not small enough to reduce the spectral leakage. On the other hand, too small r introduces too much damping into the system, which is apparent in Figure 11. For this numerical example, it is thus decided to use a compromise value of r = 1e-2.

The main reason of spectral leakage is that the amplitudes of the truncated structural responses are not low. The exponential window can be used to decay the responses. In order to determine the attenuation ratio r, structural damping is assumed to be zero, and then there is no attenuation of the simulated structural response. In this way, the attenuation is determined only by the attenuation ratio r. Hammer excitation in Figure 6 is applied in Dof 3 and DOf 6, and the accelerations of Dof 3 and DOf 5

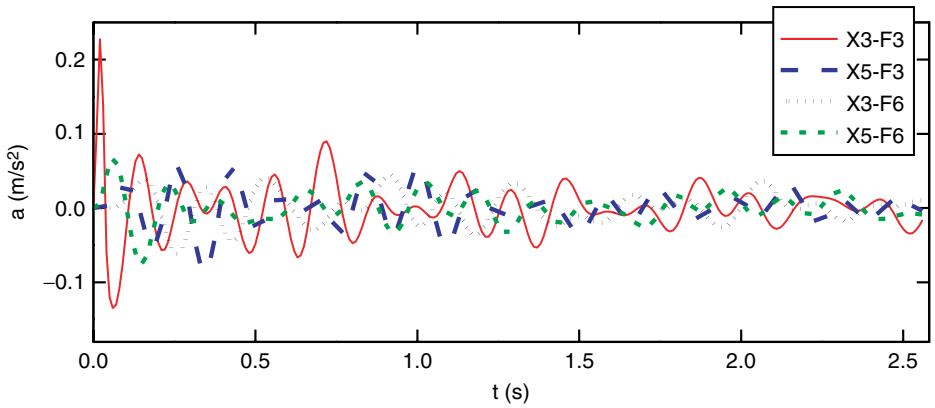

Figure 7. Responses of the global structure

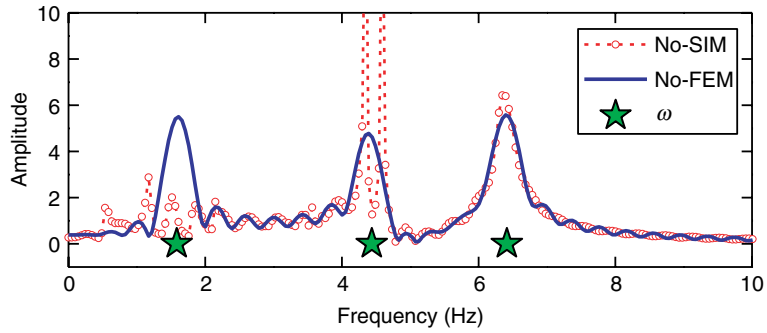

Figure 8. FRFs of the isolated substructure, no windowing: (No-SIM) constructed by the SIM; (No-FEM) computed from the FE model

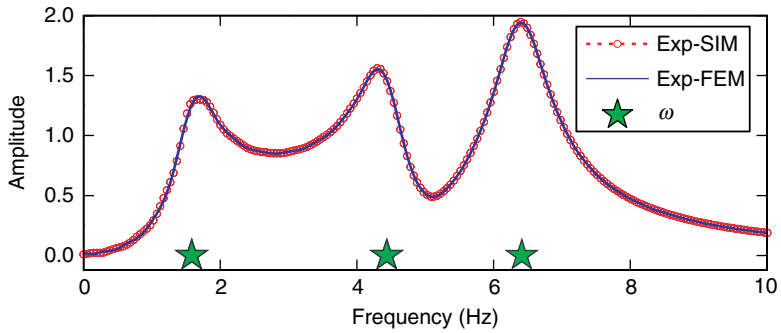

Figure 9. FRFs of the isolated substructure, exponential window: (Exp-SIM) constructed by the SIM (with r = 1e-2); (Exp -FEM) computed from the FE model

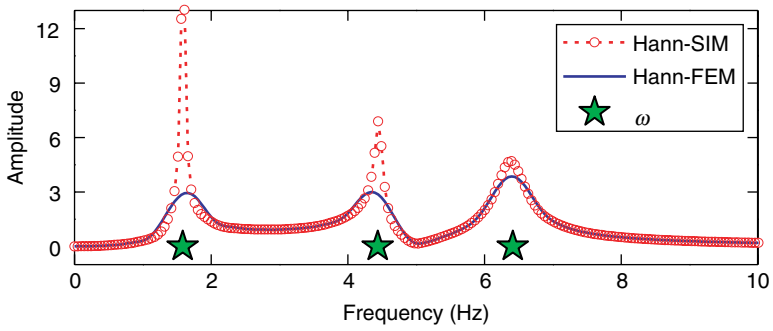

Figure 10. FRFs of the isolated substructure, Hann window: (Hann-SIM) constructed by the SIM; (Hann -FEM) computed from the FE model

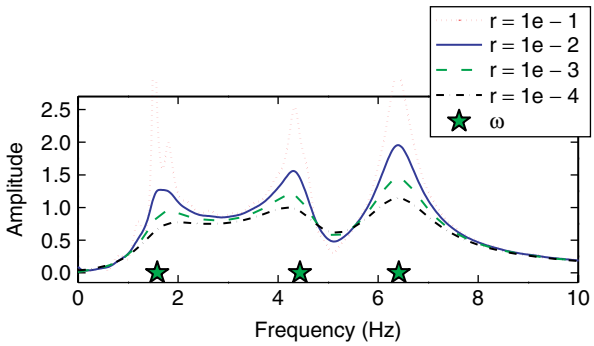

Figure 11. FRFs constructed by the SIM with the exponential window and different attenuation ratios r

are measured and used to construct the structural response of the isolated substructure. The response X5-F6 is shown in Figure 12.

First, the influence of the attenuation ratio r on the constructed isolated substructure is studied. Let $r=10^{-\alpha}$, $\alpha \in [0,3]$, and compute the nephogram of the constructed frequency response of the isolated substructure in dependence on the frequency and the attenuation ratio r (Figure 13). The dark color represents large amplitudes, that is the location of the dark color marks the eigen frequency location of the isolated substructure. The three dark lines reflect the relation between the first three frequencies of the isolated

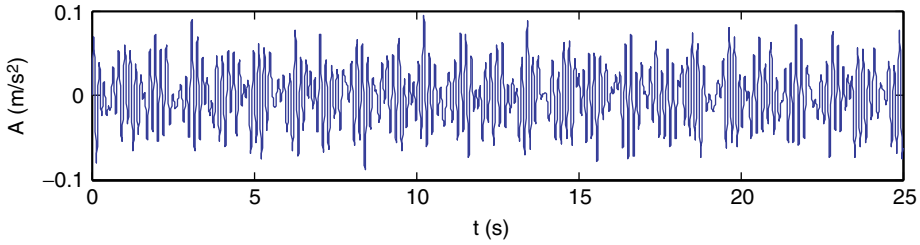

Figure 12. Responses X5-F6 of the global structure without damping

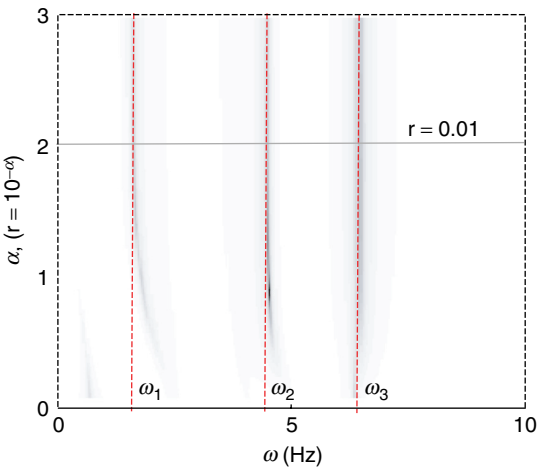

Figure 13. Nephogram of the constructed frequency response of the isolated substructure in dependence on the frequency and the attenuation ratio r

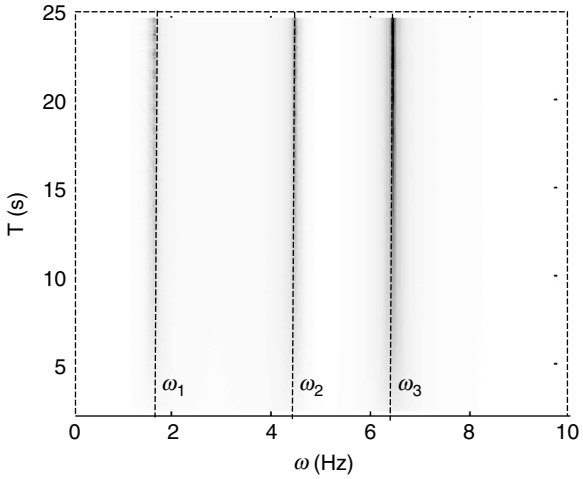

Figure 14. In case of r = 0.01, nephogram of the constructed frequency response of the isolated substructure in dependence on the frequency and time length T

substructure and the attenuation ratio r. It can be seen that the smaller value of α, i.e. the bigger value of r, corresponds to larger errors between the constructed frequency and the actual values (the dotted lines in Figure 13) of the isolated substructure. The error can be neglected when α is greater than 2, i.e. r is less than 0.01.

Then the influence of the time length T of response on the constructed isolated substructure is studied. Let $r = 0.01$, and the range of time length T be (0, 25s]. The frequency response of the isolated substructure is constructed using the measured response during time [0,T]. Figure 14 shows the nephogram of the constructed frequency response of the isolated substructure in dependence on the frequency and time length T. It can be seen that the constructed values have good accuracy. Therefore, when r = 0.01, the frequency response of isolated substructure can be constructed accurately no matter the length of the measured time.

Besides, the attenuation ratio r aims to decay the structural response, and its value can be 0.01. Therefore, in the coming experiment verification, let $r = 0.01$.

4. EXPERIMENTAL VERIFICATION

4.1. Experimental Setup

An aluminum cantilever beam is used for experimental verification. The beam is vertically suspended on a stable frame, see Figure 15(a). Its upper end is fixed to the frame, and the bottom end is either free or fixed using a "sponge support" (Figure 15(b)). The dimensions of beam is shown in Figure 16. The cross-section is 2.7 cm × 0.31 cm. Young's modulus of the beam is 70 GPa, and the density is 2700 kg/m^3. The beam is slender, so that the axial strain can be neglected; the gravity is considered: when any of the beam segments is tilted off the vertical equilibrium position, the gravity affords a certain restoring force, which is considered in the equation of motion. The upper part with the length of 79.4 cm is the substructure to be isolated and locally identified, see Figure 16. In the experiment, a segment with the length of 10.23 cm is cut evenly along its width on two sides as shown in Figure 15(c) and the dimension of the damage is shown in Figure 17. There are 15 notches on each side. The depth of each notch is 0.783 cm, and the average distance between two adjacent notches is 10.23/(15–1) = 0.73

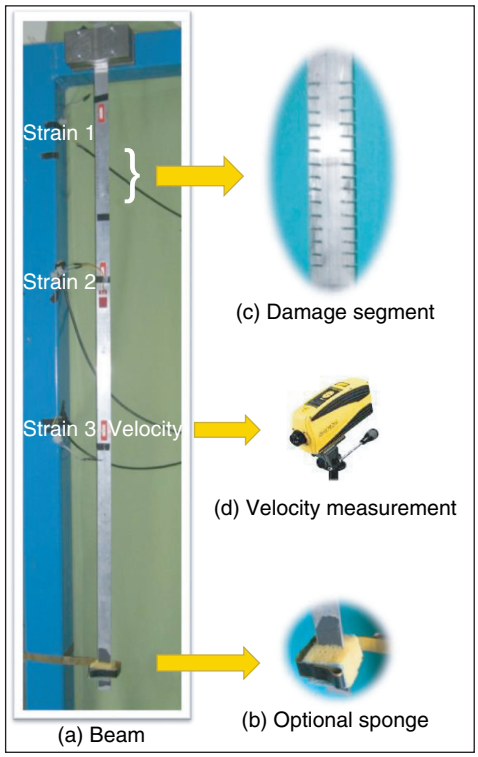

Figure 15. Cantilever beam

cm. Because notches are very narrow, the mass of the damaged section is assumed to remain unchanged. The beam width is 2.7 cm, therefore the damage factor of the damaged section is calculated as $1 - 0.783 \times 2/2.7$ 42%. Then the damaged section is taken as one of the segments to be identified.

Since the beam is slender, it is easy to excite its high natural frequencies. The FEM model of the substructure is thus densely divided into 48 elements (95 Dofs). In most other SD methods of local substructural monitoring, the full state of the substructure (in all its Dofs and at each time step) need to be computed, so that the substructure cannot have too many Dofs. In the method proposed here, the substructure can be as complex as required: only the complexity of its interface is limited by the necessity of placing sensors in the interface Dofs. As a result, application to large and complex substructures with a large number of internal Dofs is possible. A relatively dense division of the substructure into 48 elements is used to verify this point.

Three PVDF piezoelectric film sensors are placed on the substructure to measure the strain; a laser vibrometer (Figure 15(d)) is used to measure the velocity in the transverse direction. They are numbered Sensors 1 to 4, respectively. Sensor 3 ("strain3" in Figure 15(a)) and Sensor 4 ("Velocity" in Figure 15(d)) are located on the substructure interface to measure its responses.

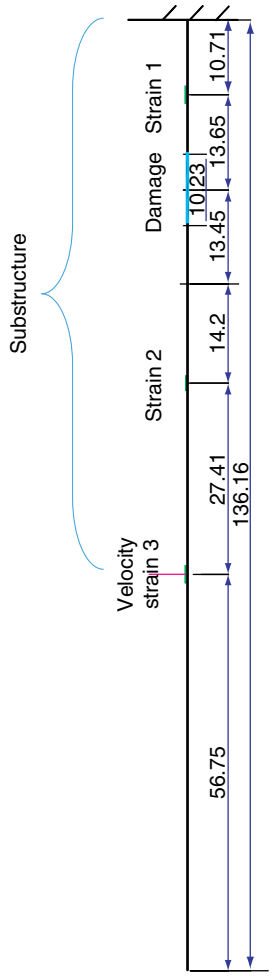

Figure 16. The dimensions of beam

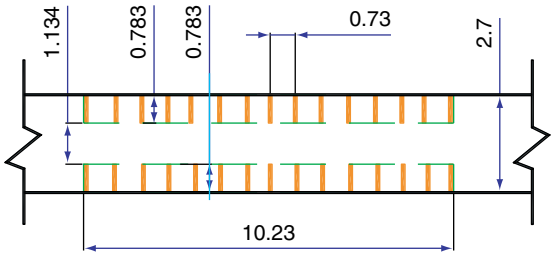

Figure 17. The dimensions of damage

Two versions of the beam are tested: the original beam with a free bottom end (beam 1) and the same beam with an additional "sponge support" on the free end (beam 2). These beams share the same substructure, hence they can be used to verify the robustness of the isolation process with respect to unknown changes of the outside structure including potential nonlinearities of beam 2 introduced by the "sponge support". All the measurements are separately performed on each of the beams.

A modal hammer is used to apply excitation in the transverse direction. Two sensors are placed on the interface, so at least three excitations need to be separately applied, including one basic excitation inside the substructure and two constraining excitations outside it. In order to make the measured responses independent of each other, the position of each excitation is limited to a different part of the beam, see Table 2. The excitation is applied by hand: note that a more accurate positioning is not required, which is a practical advantage of the method.

Since the beam is slender and light, the original FE model is built considering the gravity of the cantilever beam and the weight of the strain sensors, as well as the stiffness of the sensors. Hammer excitation knocks the beam randomly and frequencies of the beam are identified using the measured responses. Table 3 (Identified) lists the first seven identified frequencies of the intact beam and the damaged beam. The original FE model is simple, Young's modulus and the geometrical parameters are accurate, as well as the fixed end constraint. The masses and stiffnesses of the strain sensors are updated using the measured response, which is a simpler procedure not introduced here in detail. The frequencies of the updated FE model are listed in Table 3 (FEM) and compared to the identified values. Errors are computed using Eqn 22. It can be seen that the updated FE model is very accurate.

$$\varepsilon_i = \frac{\omega_i^{\mathrm{F}} - \omega_i^{\mathrm{m}}}{\omega_i^{\mathrm{m}}} \tag{22}$$

The isolated substructure has virtual supports, so it cannot be excited directly, and its natural frequencies cannot be obtained experimentally. But the FE model of the global structure is accurate and so the corresponding damaged substructure FE model is accurate, and it can be used directly for comparison with the constructed frequencies of isolated substructure.

4.2. Measured Responses

In order to obtain the necessary dynamic information of the structure, the sampling frequency of 10 kHz is used, and the measured time interval is $T = 4$ s. Two beams and three excitations are used, there are thus six groups of measured responses, see Figure 18. The legend $X(i,j,k)$ denotes the response of the ith sensor to the jth hammer excitation measured in the kth beam.

4.3. Substructure Isolation

The measured interface responses (sensors 3 and 4) are used to construct a single virtual pinned support on the interface, see Section 2.2. The corresponding FRFs of sensors 1 and 2 (as if placed in the isolated substructure) are constructed by Eqn 12. In order to confirm that the numerically isolated substructure is independent of the global structure (its constructed response is not influenced by modifications of the outside structure), responses of beam 1 are combined with responses of beam 2. Such an approach might be also convenient in practice: if the substructure is unchanged, then the measured responses can be combined with those measured in another time, no matter whether the components outside the substructure are changed or not.

Table 2. Excitations and their positions

Number	Type	Position
1	Basic excitation	Inside the substructure
2	Constraining excitation	Outside the substructure, near the interface
3	Constraining excitation	Outside the substructure, far from the interface

Table 3. The comparison of the natural frequencies

	Intact			Damaged		
Order	Identified	FEM	Error	Identified	FEM	Error
1	1.46	1.46	0.12%	1.37	1.34	-2.61%
2	8.63	8.63	0.04%	8.55	8.55	-0.09%
3	24.09	24.04	-0.20%	23.57	23.59	0.08%
4	47.14	47.08	-0.12%	44.99	44.64	-0.79%
5	77.93	77.84	-0.12%	74.65	73.39	-1.70%
6	116.31	116.29	-0.02%	113.00	112.34	-0.58%
7	162.55	162.42	-0.08%	159.00	158.79	-0.13%

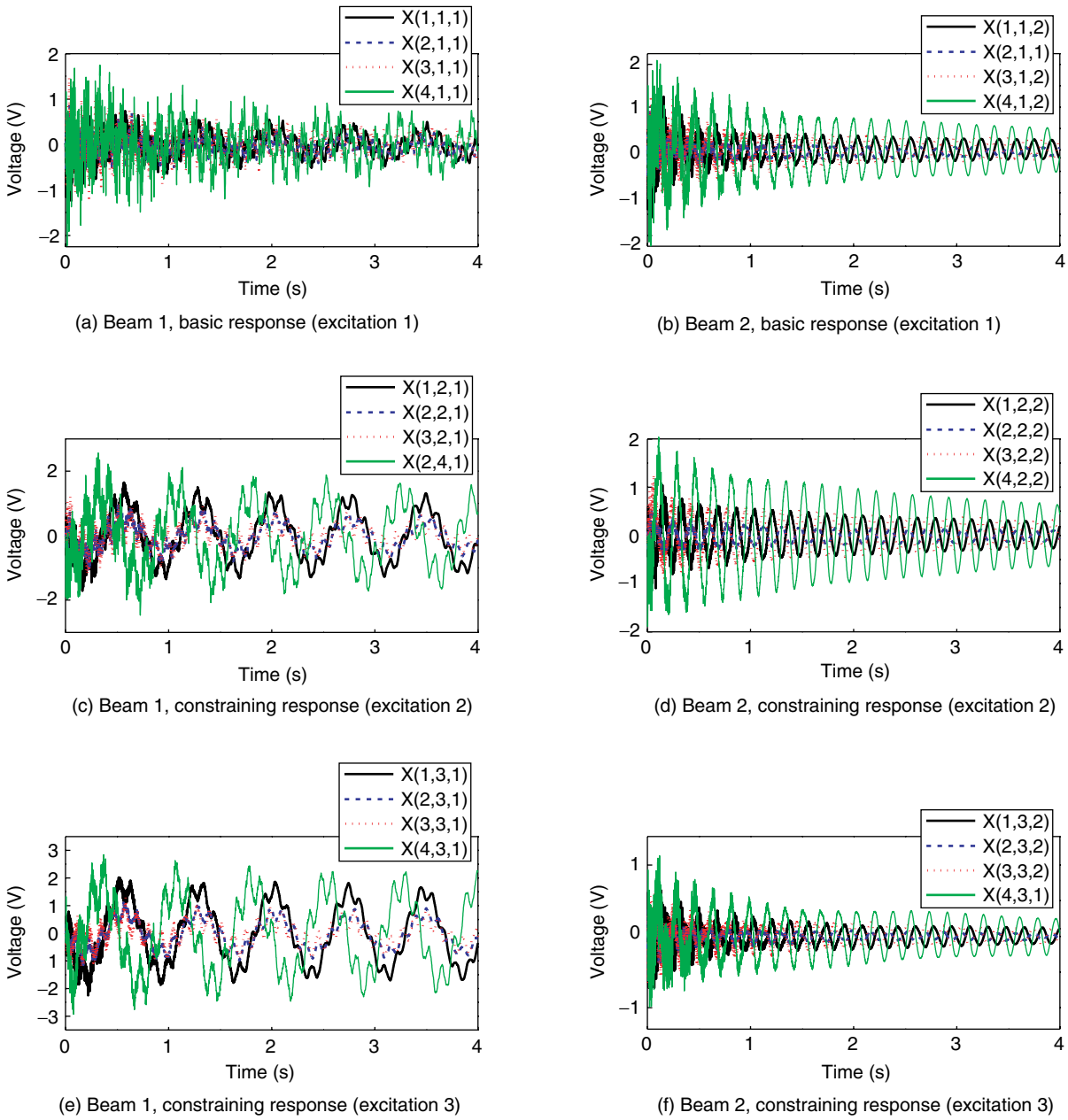

Figure 18. The measured responses of beams 1 and 2

To this end, the basic and the constraining responses measured either in beam 1 or in beam 2 can be used. There are four combinations and, consequently, the four corresponding FRFs of the isolated substructure are constructed. Their amplitudes are plotted in Figure 19, where the legend X*i*-B(*j*,*k*) denotes the FRF of the *i*th sensor in the isolated substructure constructed by using the basic responses of the *j*th beam and the constraining responses of the *k*th beam. For comparison purposes, the stars mark the natural frequencies computed using the FE model of the damaged substructure.

The attenuation ratio r in the numerical example above is adjusted by constructing frequency responses with different values of r, and the value is chosen that makes the constructed frequency response close to the actual one. Such data are not available in experimental practice, hence the value determined in the numerical example is accepted also here, that is $r = 0.01$ (decay rate $\eta = 1.5$). The peaks of the constructed FRFs (Figure 19) are obvious, and the first seven natural frequencies of the isolated substructure can be thus obtained by peak-picking. They are in good agreement with the natural frequencies computed using the FE model of the damaged substructure, see Table 4. It shows that the biggest error is 2%, and in all four cases, the constructed frequencies of the damaged isolated substructure are

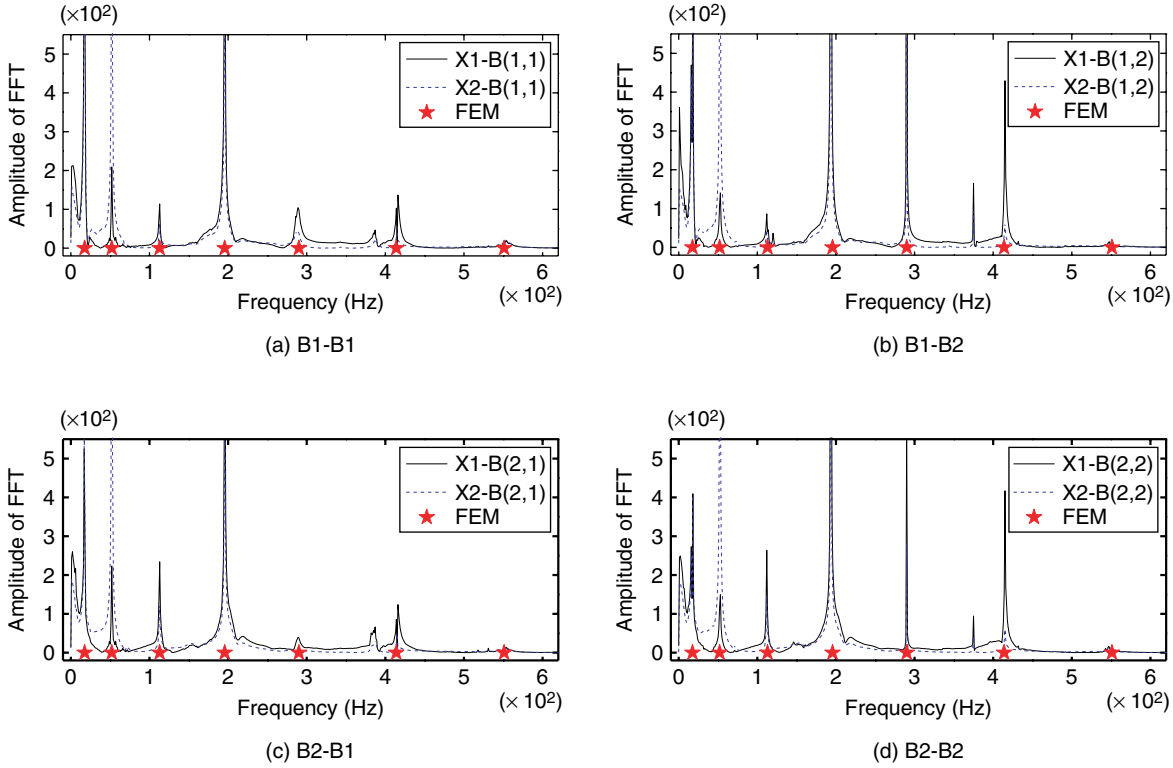

Figure 19. The four constructed FRFs of the isolated substructure

Table 4. Natural frequencies of the isolated substructure (Hz)

			Experimental identification							
	Theoretical FEM		B1-B1		B1-B2		B2-B1		B2-B2	
Order	Intact	Damaged	ω	error	ω	error	ω	error	ω	error
1	17.685	17.519	17.4	–0.68%	17.4	–0.68%	17.2	–1.85%	17.2	–1.85%
2	57.332	52.007	52.4	0.75%	52.4	0.75%	52.6	1.13%	52.6	1.13%
3	119.154	112.949	112.7	–0.22%	112.8	–0.13%	112.5	–0.40%	111.5	–1.30%
4	203.297	195.661	195.7	0.02%	195.7	0.02%	193.3	–1.22%	192.4	–1.69%
5	310.471	290.037	288	–0.71%	289	–0.36%	289.3	–0.25%	289.2	–0.29%
6	439.947	413.933	415	0.26%	416	0.50%	416.5	0.62%	416.2	0.54%
7	592.476	551.067	553	0.35%	553	0.35%	546.8	–0.78%	546.7	–0.80%

close to those of its FE model, which proves that the isolated substructure is constructed accurately. In all four combination cases, the identified natural frequencies are similar, which confirms that the isolation process is independent of the outside structure: if the substructures are the same, the constructed isolated substructures are also the same, no matter the outside that can be unknown, nonlinear or changing.

4.4. Identification of the Isolated Substructure

The substructure is divided into five segments, see Figure 20, where each segment contains 9 or 10 finite elements. The second segment is actually damaged, so that the

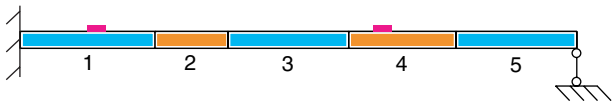

Figure 20. Division of the substructure into five segments

actual damage extents of the five segments are $[1\ 0.42\ 1\ 1\ 1]^T$. The damages of the substructure are identified by minimizing the square distance (Eqn 15) between the constructed natural frequencies of the isolated substructure and the natural frequencies computed using its FE model. The damages are identified with a good accuracy in all four combination cases, see Figure 21 and

Table 5. The proposed method performs well with a substructure with 95 Dofs, which makes it a substructure significantly more complex than the substructures used in most other SD methods of local substructural monitoring.

5. DISCUSSION

5.1. Time-Domain and Frequency-Domain Method

This paper proposes a frequency-domain method of substructure isolation. In comparison to the time-domain method (Hou *et al*. 2012), it is computationally significantly more efficient, which is one of its main advantages. Let n be the number of the constraining excitations (interface sensors), and denote by n_t the number of the time steps. Since the number of spectral lines after the FFT is proportional to the number of the time steps, and for each spectral line a pseudoinverse of an $n \times n$ matrix needs to be computed, the time complexity of the frequency-domain method, including the cost of the FFT, is $O\left(n^3 n_t + n n_t \log n_t\right)$. The isolation in time-domain requires a single computation of the pseudoinverse of a large $n_t n \times n_t n$ matrix, which yields a significantly higher time complexity of $O\left(n^3 n_t^3\right)$. For example, the measurement time interval considered in this experiment is 4 s, while for the time-domain method it is only 0.4 s (at the same sampling rate). Despite the ten times longer time interval, the frequency-domain method is approximately six orders of magnitude faster.

In terms of accuracy, there is no significant difference between the damage extents identified here (Figure 16) and the damage extents identified using the time-domain approach and the same objective function (Figure 18, Hou *et al*. 2012).

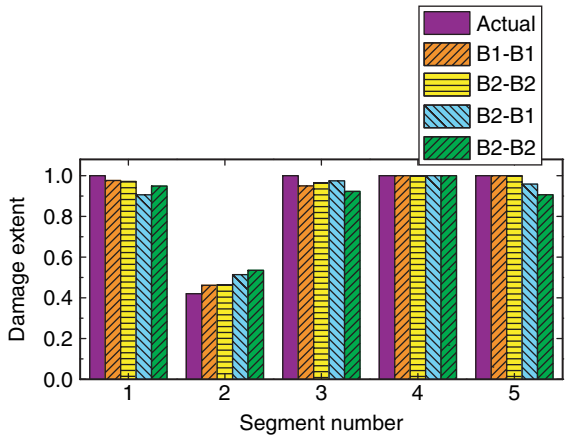

Figure 21. The identified damage extents of the substructure

5.2. Constraining Excitations

The matrix $B(\omega)$ in Eqn (12) consists of structural responses to constraining excitations. To avoid excessive ill-conditioning, the correlation between its columns should be as close to zero as possible. However, if closely-spaced, similar constraining excitations are used, then the corresponding responses are also similar and the correlation is high. Therefore, essentially different constraining excitations should be used; in this example, they are applied in different positions with a certain distance from each other.

5.3. Substructure Interface and Constraining Sensors

Two factors need to be considered in practical application of the method. The first is the selection of the substructure, which should have a simple interface with the outside global structure. The second is the selection of the constraining sensors and their location on the interface: it depends on the intended type of the virtual supports, which should ensure that the constructed response of the isolated substructure is sensitive to the local information being identified.

Table 5. Identified damage extents of the substructure and their absolute errors

Segment number		1	2	3	4	5
Actual damage		**1.000**	**0.420**	**1.000**	**1.000**	**1.000**
B1-B1	Identified	0.976	0.462	0.950	1.000	1.000
	Error	–2.36%	4.15%	–5.02%	0.00%	0.00%
B1-B2	Identified	0.972	0.463	0.966	1.000	1.000
	Error	–2.85%	4.32%	–3.44%	0.00%	0.00%
B2-B1	Identified	0.906	0.514	0.975	1.000	0.959
	Error	–9.39%	9.40%	–2.54%	0.00%	–4.14%
B2-B2	Identified	0.949	0.535	0.923	1.000	0.906
	Error	–5.11%	11.50%	–7.72%	0.00%	–9.38%

6. CONCLUSIONS

This paper extends the substructure isolation method (SIM) into frequency domain (SIM-FD). The efficiency and accuracy of the approach are verified using a mass-spring numerical model and a beam experiment. The method focuses on local damage identification of the substructure, so that, in contrast to other substructuring methods, unknown interface forces (damping coefficients, state vectors, etc.) do not need to be identified. Therefore, damage parameters are the only unknowns, so that local identification can be generally easier and numerically more stable. It is an advantage in applications to substructures that feature a larger number of internal Dofs. The proposed SIM-FD transfers the isolation process from time domain into frequency domain. The isolated substructure can be constructed separately for each frequency of interest, which significantly decreases the numerical costs of isolation. During the isolation process, selection of the windowing function for the FFT is important. The exponential window is suggested, which avoids the spectral leakage and preserves the frequency information of the isolated substructure.

The SIM requires the interface responses to be measured in order to construct the virtual supports. In complex boundary conditions, it may restrict the applicability of the method. This limitation is a subject of an ongoing research.

ACKNOWLEDGEMENTS

The authors gratefully acknowledge the support of the Major State Basic Research Development Program of China (973 Program)(2013CB036305), of National Science Foundation of China (NSFC) (51108057, 51108066), of the Fundamental Research Funds for the Central Universities(China) (DUT13LK13), of Special Financial Grant from the China Postdoctoral Science Foundation (2012T50255), and of the Project of National Key Technology R&D Program (China) (2011BAK02B01, 2011BAK02B03, 2006BAJ03B05). Financial support of the Polish National Science Centre Project "AIA" (DEC-2012/05/B/ST8/02971) and the FP7 EU project Smart-Nest (PIAPP-GA-2011-28499) is gratefully acknowledged.

REFERENCES

An, Y. and Ou, J. (2013). "Experimental and numerical studies on model updating method of damage severity identification utilizing four cost functions", *Structural Control and Health Monitoring*, Vol. 20, No. 1, pp. 107–120.

Bao, Y., Li, H., An, Y. and Ou, J. (2012). "Dempster–Shafer evidence theory approach to structural damage detection", *Structural Health Monitoring*, Vol. 11, No. 1, pp. 13–26.

Duan, Z., Yan, G., Ou, J. and Spencer, B.F. (2005). "Damage localization in ambient vibration by constructing proportional flexibility matrix", *Journal of Sound and Vibration*, Vol. 284, No. 1-2, pp. 455-466.

Ewins, D.J. (2000). *Modal Testing, Theory, Practice, and Application,* 2nd ed, Research Studies Press, England.

Fan, W. and Qiao, P. (2011). "Vibration-based damage identification methods: A review and comparative study", *Structural Health Monitoring*, Vol. 10, No. 1, pp. 83-111.

Hassiotis, S. (2000). "Identification of damage using natural frequencies and markov parameters", *Computers and Structures*, No. 74, pp. 365–373.

Harris, F.J. (1978). "On the use of windows for harmonic analysis with the discrete Fourier transform", *Proceedings of the IEEE*, Vol. 66, No. 1, pp. 51–83.

Hou, J., Jankowski, Ł and Ou, J. (2012). "Experimental study of the substructure isolation method for local health monitoring", *Structural Control and Health Monitoring*, Vol. 19, No. 4, pp. 491–510.

Kim, H. and Melhem, H. (2003). "Fourier and wavelet analyses for fatigue assessment of concrete beams", *Experimental Mechanics*, Vol. 43, No. 2, pp. 131–140.

Koh, C.G. Hong, B. and Liaw, C.Y. (2003). "Substructural and progressive structural identification methods", *Engineering Structures*, Vol. 25, No. 12, pp. 1551–1563.

Kress R. (1989). *Linear Integral Equations. In: Applied Mathematical Sciences*, Vol 82, Springer, New York.

Law, S.S. and K. Zhang, Duan, Z.D. (2010). "Structural damage detection from coupling forces between substructures under support excitation", *Engineering Structures*, Vol. 32, No. 8, pp. 2221–2228.

Lin, R.M. and Ewins, D.J. (1990). "Model updating using FRF data", *15th Int. Seminar on Modal Analysis*, Leuven, Belgium, pp. 141-162.

Maia, N. and Silva, J. (1997). *Theoretical and Experimental Modal Analysis*, Research Studies Press, England.

Moragaspitiya, H., Thambiratnam, D., Perera, N. and Chan, T. (2012). "Health monitoring of buildings during construction and service stages using vibration characteristics", Advances in Structural Engineering. Vol. 15, No. 5, pp. 717–726.

Nair, K.K., Kiremidjian, A.S., Lei, Y., Lynch, J.P. and Law, K.H. (2003). "Application of time series analysis in structural damage evaluation", *International Conference on Structural Health Monitoring,* Tokyo, Japan.

Rucka, M. and Wilde, K. (2010). "Neuro-wavelet damage detection technique in beam, plate and shell structures with experimental validation", *Journal of Theoretical and Applied Mechanics*, Vol. 48, No. 3, pp. 579–604.

Suwała, G. and Jankowski, Ł. (2012). "A model-free method for identification of mass modi_cations", *Structural Control and Health Monitoring*, Vol. 19, No. 2, pp. 216–230.

Tee, K.F., Koh, C.G. and Quek, S.T. (2005). "Substructural first- and second-order model identification for structural damage

assessment", *Earthquake Engineering & Structural Dynamics*, Vol. 34, No. 15, pp. 1755–1775.

Tee, K.F., Koh, C.G. and Quek, S.T. (2009). "Numerical and experimental studies of a substructural identification strategy", *Structural Health Monitoring*, Vol. 8, No. 5, pp. 397–410.

Trinh, T.N. and Koh, C.G., (2012). "An improved substructural identification strategy for large structural systems", *Structural Control and Health Monitoring*, Vol. 19, No. 8, pp. 686–700.

Wang, X.J., Zhou, X., Xia, Y., Weng, S. (2013). "Comparisons between modal-parameter-based and flexibility-based damage identification methods", *Advances in Structural Engineering*, Vol. 16, No. 9, pp. 1611–1620.

Wang, X.J., Koh, C.G. and Zhang, Z. (2011). "Damage identification based on strain and translational measurements with substructure approach", *1st Middle East Conference on Smart Monitoring, Assessment and Rehabilitation of Civil Structure*, Dubai, UAE.

Xia, Y. Chen, B., Weng, S., Ni, Y.Q. and Xu, Y.L. (2012), "Temperature effect on vibration properties of civil structures: A literature review and case studies", *Journal of Civil Structural Health Monitoring*, Vol. 2, No. 1, pp. 29–46.

Xia, Y. and Weng, S., Xu, Y.L. and Zhu, H.P. (2010). "Calculation of eigenvalue and eigenvector derivatives with the improved Kron's substructuring method", *Structural Engineering and Mechanics*, Vol. 36, No. 1, pp. 37–55.

Xing, Z. and Mita, A., (2012). "A substructure approach to local damage detection of shear structure", *Structural Control and Health Monitoring*, Vol. 19, No. 2, pp. 309–318.

Yi, J., Kim, D., Go, M., Kim, J., Park, J., Feng, M. and Kang, K. (2012). "Application of structural health monitoring system for reliable seismic performance evaluation of infrastructures", *Advances in Structural Engineering*, Vol. 15, No. 6, pp. 955-968.

Yuen, K.V. and Katafygiotis, L.S. (2006). "Substructure identification and health monitoring using noisy response measurements only", *Computer-Aided Civil and Infrastructure Engineering*, Vol. 21, No. 4, pp. 280–291.

Yun, C.B. and Bahng, E.Y. (2000). "Substructural identification using neural networks", *Computers and Structures*, Vol. 77, No. 1, pp. 41–52.

Zhang, D., DeVore, C. and Johnson, E.A. (2010). "Experimental verification of controlled substructure identification for shear structures", *5th World Conference on Structure Control and Monitoring (5WCSCM)*, Tokyo, Japan.

Zhou, L.R., Yan, G.R. and Ou, J.P. (2013), "Response surface method based on radial basis functions for modeling large-scale structures in model updating", *Computer-Aided Civil and Infrastructure Engineering*, Vol. 28, No. 3, pp. 210–226.

Zhou, L.R., Yan, G.R., Wang, L., Ou, J.P. (2013). "Review of benchmark studies and guidelines for structural health monitoring", *Advances in Structural Engineering*, Vol. 16, No. 7, pp. 1187–1206.

Zhu, H.P., Mao, L., Weng, S. (2013). "Calculation of dynamic response sensitivity to substructural damage identification under moving Load", *Advances in Structural Engineering*, Vol. 16, No. 9, pp. 1621–1632.